

We are IntechOpen, the world's leading publisher of Open Access books Built by scientists, for scientists

4,800

Open access books available

122,000

International authors and editors

135M

Downloads

Our authors are among the

154

Countries delivered to

TOP 1%

most cited scientists

12.2%

Contributors from top 500 universities



WEB OF SCIENCE™

Selection of our books indexed in the Book Citation Index
in Web of Science™ Core Collection (BKCI)

Interested in publishing with us?
Contact book.department@intechopen.com

Numbers displayed above are based on latest data collected.
For more information visit www.intechopen.com



Applications of Synchrotron-Source IR Spectroscopy for the Investigation of Insect Wings

Samuel Cheeseman, Vi Khanh Truong, Jitraporn Vongsvivut, Mark J. Tobin, Russell Crawford and Elena P. Ivanova

Abstract

Synchrotron-source infrared (IR) spectroscopy offers an effective method to characterise the chemical composition across surfaces. The intense light source allows the detection of trace quantities of different chemical components with a superior signal-to-noise ratio, while the highly collimated light enables high-resolution spatial mapping of the chemical distribution. In this chapter, we introduce synchrotron-source IR spectroscopy, using the infrared microspectroscopy (IRM) beamline at the Australian Synchrotron as an example. We then discuss the use of synchrotron-source IR spectroscopy to analyse insect wings in terms of experimental setup and a summary of the results in two different modes of operation, transmission and attenuated total reflection (ATR). Insect wings possess unique anti-wetting, self-cleaning, anti-biofouling and bactericidal properties and provide inspiration for biomimetic surfaces on synthetic materials which possess similar properties, useful in a range of industries.

Keywords: synchrotron, infrared, insect wings, IR spectroscopy, FTIR

1. Introduction

Infrared (IR) spectroscopy can be used for the chemical characterisation and identification of materials. The use of a synchrotron light source, which is extremely intense and highly collimated, enables a superior signal-to-noise ratio and high-resolution spatial mapping of materials and surfaces compared to alternative IR sources.

IR spectroscopy relies on the absorption of specific wavelengths within the IR spectra, upon interacting with certain molecular bonding. Differences in electronegativity and/or orientations of molecular species create a disproportional distribution of charges. Atomic elements that are more electronegative more strongly attract electrons when bonding with an element with lower electronegativity, resulting in dipole moments. As the molecules naturally vibrate, the distance between the negative charge centre of each elemental species in a specific bond fluctuates, creating an electric field. This fluctuation is known as the resonant frequency. If the frequency of the IR radiation, which changes according to wavelength, matches the molecular resonant frequency, the radiation is absorbed. The size of the molecular frequency is determined by the size and electronegativity of the atoms involved in the chemical bond, as well as the immediate molecular

environment. These modes of vibration can include bending, scissoring, rocking and symmetric and asymmetric stretching [1]. Through detection of absorbed wavelength ranges, which typically form easily identifiable peaks, it is possible to determine the major chemical bonding present in the sample, indicative of the chemical composition [2, 3].

This chapter discusses the setup, advantages and results of synchrotron-source IR spectroscopy for the investigation of insect wings, with a particular focus on the setup at the Australian Synchrotron. The wings of particular insects are of interest as they possess unique anti-wetting, anti-biofouling and mechano-bactericidal properties due to their chemical composition and nanostructured surface [4–8]. These properties are useful as biomimetic templates for the design of anti-wetting and anti-biofouling materials, with applications in a range of industries such as the hulls of ships or water pipes [9]. Additionally, the mechano-bactericidal activity of these surfaces provide a novel solution to preventing bacterial colonisation on biomedical devices and other surfaces, particularly in light of emerging concerns of antibiotic resistance. These surfaces are advantageous to present strategies which rely largely on coatings embedded with antimicrobial agents resulting in issues of reduced efficacy over time and cytotoxic side effects and can promote the development of resistance [10–13].

2. Infrared beamline at the Australian Synchrotron

Infrared (IR) microspectroscopy, as the name suggests, allows the chemical composition of materials to be determined at the microscopic scale. Typically, an IR transmission microscope, with all reflecting optics, is coupled to a Fourier-transform IR (FTIR) spectrometer, permitting mid-IR absorption spectra to be collected from features as small as 5–10 μm in size within a sample to be analysed or identified. This process relies on the use of a high numerical aperture (NA) condenser and objective optics to focus the IR beam onto the sample, with the subsequent collection of the beam that has passed through the sample. The limit of the sample dimensions that can be examined is set by the optical diffraction limit at the analysing wavelength (e.g. $1600\text{ cm}^{-1} = 6.25\text{ }\mu\text{m}$ in wavelength). Selection of the region of interest for analysis is typically determined by inserting an aperture into the optical path of the IR beam at a focus position that is placed either before or after the sample. This results in a loss of most of the intensity of the beam from a conventional IR source, such as that of a Globar™ source, from reaching the detector. Alternatively, multi-pixel IR imaging detectors, such as linear array and focal plane array (FPA) detectors, can be used to enable the simultaneous collection of FTIR spectra from many positions within the sample. This approach, however, also typically relies on less than 0.1% of the total intensity of the IR source being directed to each sensing element of the FPA detector.

An alternative approach, described here, combines the high brightness of a broadband synchrotron source with an FTIR spectrometer and IR microscope, which enables the full intensity of the IR source to be directed to a diffraction-limited position on the sample. This results in a high signal intensity and a high signal-to-noise ratio (SNR) when analysing samples with features of 5–10 μm in size [14–16]. Synchrotron IR beamlines dedicated to the high spatial resolution analysis of microscopic materials are currently in operation at a number of national laboratories worldwide.

The Australian Synchrotron commenced operations for researchers in 2007, with two IR beamlines having been included in the initial suite of beamlines. One of these was dedicated to high spectral resolution gas-phase spectroscopy in the far-IR spectral region, while the other beamline was established for mid-IR

microspectroscopy. Extraction of IR radiation from the Australian Synchrotron is achieved through the incorporation of a removable plane mirror (M1, see **Figure 1**) within the vacuum chamber of one of the dipole bending magnets of the electron storage ring. **Figure 1A** shows the modified vacuum chamber of the electron storage ring, with two ports incorporated to enable the insertion of the IR M1 mirror and extraction of the IR light reflected off the M1 mirror. **Figure 1B** shows the M1 mirror undergoing vibration testing prior to installation in the synchrotron storage ring. When inserted, the M1 mirror collects an angular portion of the emitted IR and visible synchrotron radiation of 58 mrad (horizontal) and 17 mrad (vertical), with this beam being reflected towards a toroidal focusing mirror (M2). This mirror focuses the beam downwards towards two plane mirrors M3 and M3a, which, in turn, direct the beam to a focus point through the shield wall at a position just beyond a chemical vapour deposition (CVD) diamond window that separates the vacuum of the synchrotron storage ring from the vacuum of the IR beamlines.

A schematic depiction of the beamline layout is given in **Figure 1C**. Beyond the CVD diamond window, the synchrotron beam expands and is directed to the beam splitter optics, where half of the horizontal fan of radiation is reflected to each of the two IR beamlines. The final matching optics for each of the IR beamlines is designed to provide a well-collimated beam that is matched in dimensions to the internal optics of the FTIR instrument, which is coupled to the beamline. In the case of the IR microspectroscopy (IRM) beamline, a combination of plane mirrors and a spherical focusing mirror delivers a collimated beam of approximately 12 mm × 12 mm in an area at the entrance port of the FTIR spectrometer. While this beam does not fill the interferometer beam splitter, it provides a beam that is matched in size to the entrance aperture of the reflecting condenser optic used for most experiments.

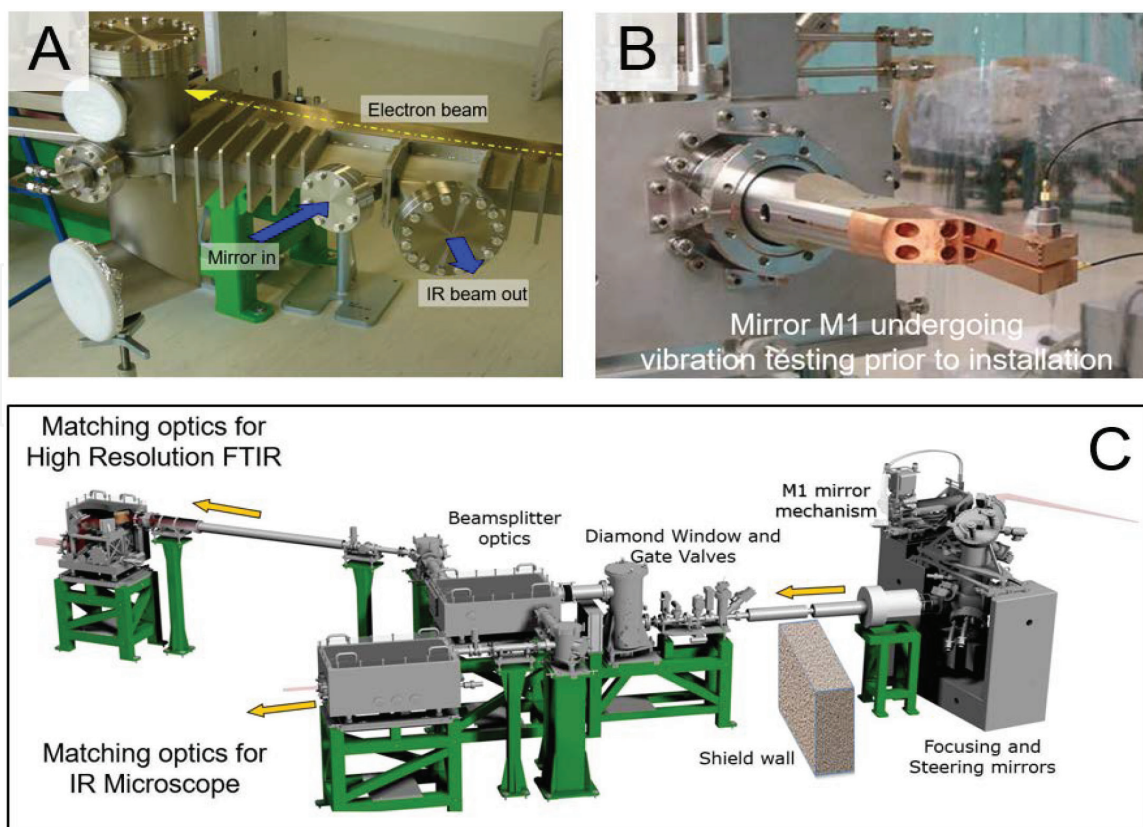


Figure 1. (A) Modified vacuum chamber of the storage ring dipole magnet, with ports to allow the insertion of the M1 beamline mirror and the collection of the reflected radiation. (B) M1 mirror undergoing vibration testing. (C) Layout of the beamline optics of the IRM and THz/far-IR beamlines and their shared beamline front end.

3. Experimental setup for the investigation of insect wings

The IRM beamline at Australian Synchrotron is equipped with a Bruker VERTEX 80v FTIR spectrometer coupled with a Hyperion 2000 FTIR microscope and a liquid nitrogen-cooled narrowband mercury cadmium telluride (MCT) detector (Bruker Optik GmbH, Ettlingen, Germany). The synchrotron FTIR mapping measurements described in this chapter were performed within a spectral range of 3800–700 cm^{-1} using a 4 or 8 cm^{-1} spectral resolution. Blackman-Harris 3-Term apodisation, Mertz phase correction and zero-filling factor of 2 were set as default acquisition parameters using OPUS software suite (Bruker).

There are several operation modes available at the beamline, depending on the specific requirements of the experiment. The primary modes of operation are transmission, reflectance, transmittance, grazing incidence reflectance and attenuated total reflection (ATR). Transmission microspectroscopy generally requires the samples to be thinner than $\sim 10 \mu\text{m}$, whereas reflectance and transmittance measurements ideally require the sample to be highly polished or placed on a reflective substrate such as gold or on low-emissivity (low-E) slides. Grazing incidence reflectance can be applied to the study of thin films on metallic surfaces, while ATR microspectroscopy can be applied to a diverse array of samples ranging from soft gels [17], fingerprints [18] and food products [19] to single fibres [20] and composite materials [21, 22]. Details of the experimental setups for transmission and ATR measurements, which are the two main operation modes used for the investigation of insect wings, are given below.

3.1 Transmission

Prior to spectral data acquisition, the preparation of insect wing samples involves the dissection of the wing membrane into rectangular sections of approximately 5 mm \times 8 mm in area using a surgical blade. The wing sections were then gently rinsed with MilliQ H_2O (resistivity of 18.2 $\text{M}\Omega \text{cm}^{-1}$, Merck Millipore, Washington, DC, USA) and then blow-dried using 99.99% purity nitrogen gas [23–26].

For transmission measurements, the wing sections were held on a gap between an aluminium support frame using polyimide (Kapton[®]) tape to fix both sides of the section, before being transferred onto the sample stage of the microscope (**Figure 2A**). The IR microscope was operated with a matching 36 \times IR reflecting objective and condenser (NA = 0.5). In transmission mode, the synchrotron IR beam passes through a condenser located below the microscope stage and is focused into a small spot onto the wing sample (**Figure 2B**). By coupling the IR microscope to a synchrotron source, significant advantages could be gained regarding the highly collimated and highly intense synchrotron IR beam, particularly for single point FTIR microanalysis of sampling areas in the order of 3–5 μm^2 . At the IRM beamline, the area of measurement per pixel on the sample is defined by the size of a single aperture located in a focal plane between the sample and detector, which can be adjusted to be as small as 4–5 μm , whereas the minimum step interval between pixels allowed for this microscope is 1 μm . Therefore, synchrotron FTIR microspectroscopy has been proven to be a powerful analytical tool for acquiring the spatially resolved distribution of chemical functional groups present across selected areas of the insect wings being analysed [14, 23–26].

3.2 Attenuated total reflection (ATR)

ATR-FTIR spectroscopy utilises the property of total internal reflection, which is established when light travelling in an optically denser medium of an ATR crystal element impinges onto the surface of a lower-index medium with an incident angle

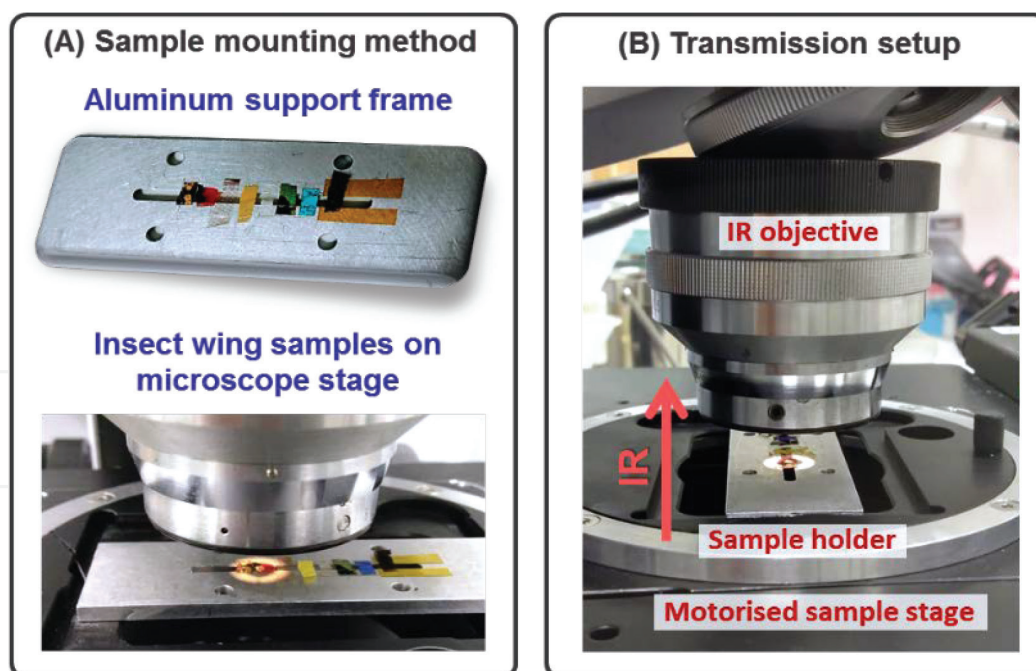


Figure 2.
(A) An aluminium support frame used as a sample holder for mounting insect wing sections prior to them being transferred onto the microscope stage and (B) schematic diagram showing the IR beam path in transmission mode for the investigation of insect wings.

greater than the critical angle [27]. Under these specific conditions, the electromagnetic field (i.e. an evanescent wave) penetrates and decays exponentially within a shallow depth of the adjacent low-index sample. Any IR-absorbing material located in contact with this interface interacts with the evanescent field resulting in an IR absorption, which is consequently transformed into an ATR-FTIR spectrum. The typical path lengths that the evanescent wave penetrates into most organic samples range from 0.2 μm to 5 μm , depending on the refractive indices of the ATR crystal and the sample, the angle of incidence and the wavelength of light [27]. As a result, the ATR-FTIR technique has been widely used for probing surface-specific molecular information of materials. The technique has been used as an alternative sampling method (i) when the sample cannot be prepared as thin sections for transmission measurements and (ii) to avoid scattering artefacts commonly presented in transmittance measurements.

Two models of ATR devices were developed for mapping measurements at the IRM beamline based on the use of an ATR hemispherical element known as the macroscopic (macro) ATR-FTIR technique [17, 28]. The technique increases the field of view and only requires a single contact point for the entire mapping measurement, preventing the cross contamination between measurement points and minimising the sample damage, which often occur in the traditional microscopic (micro) ATR-FTIR approach where repeated contacts are performed similar to a tapping mode.

While one of the ATR models was developed based on a piezo-controlled driving system [17], the so-called “hybrid” macro ATR-FTIR, which is the main ATR device used for the analysis of insect wings, was developed by modifying the cantilever arm of a standard Bruker macro ATR-FTIR unit to accept germanium (Ge) ATR elements with different facet sizes (i.e. 1 mm, 250 μm and 100 μm in diameter) to suit for different types of sample surfaces (**Figure 3A**). Coupling the synchrotron IR beam to the Ge ATR hemispherical crystal ($n_{\text{Ge}} = 4$) using a high NA microscope objective essentially reduces (i) the beam focus size and (ii) the mapping step size (relative to the stage step motion) by a factor of 4, hence further improving the spatial resolution when compared to transmission or transmittance microspectroscopy. As a result, synchrotron macro ATR-FTIR measurements can be performed

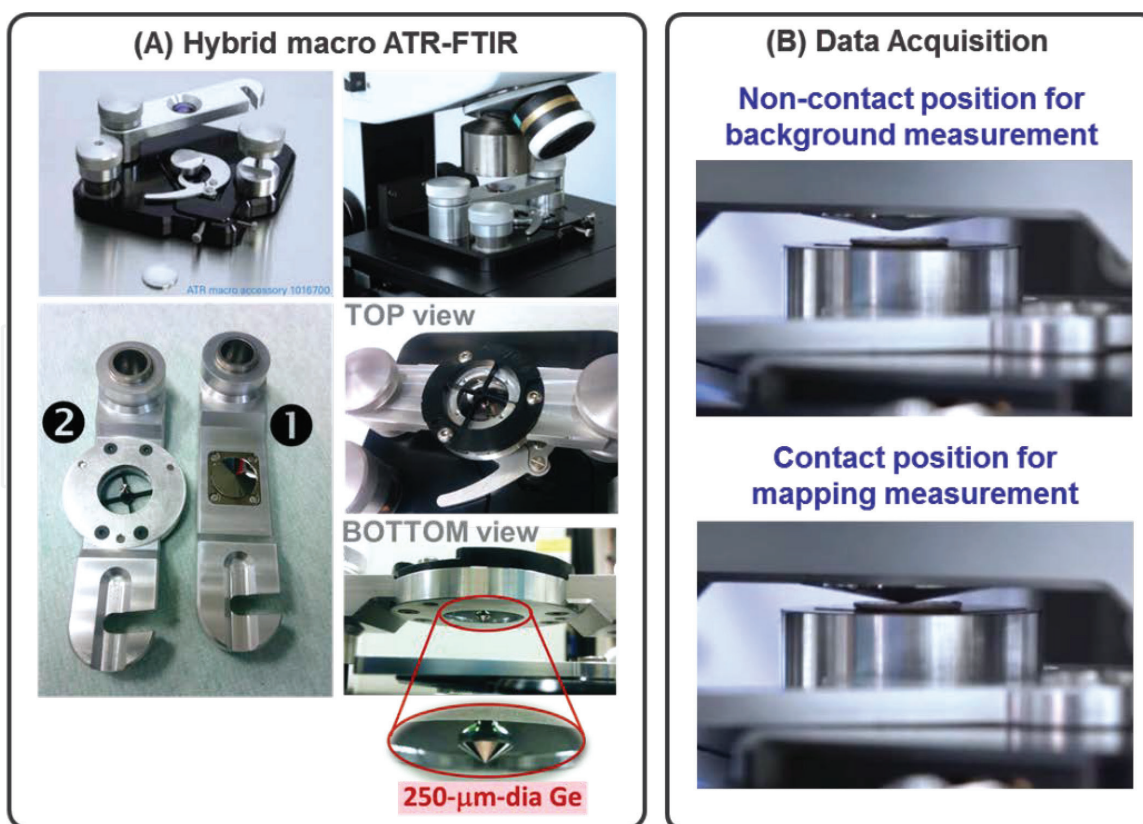


Figure 3.

(A) Hybrid macro ATR-FTIR device, showing the standard macro ATR-FTIR unit (top) and the adaptation of the cantilever arm to couple with the smaller diameter Ge micro-ATR crystal (2) compared to the original 1 mm diameter Ge macro ATR crystal (1) (bottom) and (B) data acquisition process involving background measurement of air in the noncontact position followed by mapping measurement of the wing sample in the contact position.

with aperture sizes that are 4 times larger, thereby eliminating the diffraction effects introduced by small aperture dimensions, making it ideal for high-resolution chemical analysis.

In practice, the wing section was mounted on an aluminium disc using polyimide (Kapton[®]) tape to hold both sides of the wing. The aluminium disc was then placed into the sample stage of the macro ATR-FTIR unit. As illustrated in **Figure 3B**, the Ge ATR crystal was subsequently brought to the focus of the synchrotron IR beam, and a background spectrum was recorded in air using 4 or 8 cm⁻¹ spectral resolution and 256 co-added scans. After that, the wing sample was brought into contact with the Ge ATR crystal, and a synchrotron macro ATR-FTIR chemical map was acquired using shorter co-added scans (such as 8, 16 or 32 scans) depending on the observed absorption intensity and the quality of the contact. With the use of a Ge ATR crystal ($n_{\text{Ge}} = 4$), the area of measurement per pixel on the wing sample can be as small as 1.9 μm, and the minimum step interval between pixels achievable is 0.25 μm.

The use of synchrotron-source infrared (IR) spectroscopy is an effective method of surface characterisation to determine the chemical composition across insect wings. The intense and highly collimated light source allows sensitive detection of chemical components with high-resolution spatial mapping.

4. Case study: investigation and characterisation of insect wings

The wings of some insects exhibit unique anti-wetting, anti-biofouling, self-cleaning and bactericidal properties, primarily due to nanostructured arrays of lipids on the wing epicuticle [4–8]. These properties are of interest as a biomimetic template for

the design of anti-biofouling and self-cleaning surfaces, with applications in a range of industries [9]. Additionally, the mechano-bactericidal activity of these surfaces provides a novel solution to preventing bacterial colonisation on biomedical devices and other surfaces, particularly in light of emerging concerns of antibiotic resistance. This bactericidal activity was first discovered on the wings of cicadas and shortly after dragonflies and damselflies and has since been successfully extended to synthetic analogues of the wings, with similar high aspect ratio nanoscale features [5, 29–31]. These surfaces present advantages over traditional strategies that typically rely on coatings embedded with antimicrobial agents, which can have issues of reduced efficacy over time and cytotoxic side effects and promote the development of resistance [10–13].

The wing membrane of these insects can be broken into two primary components, the procuticle and the epicuticle (**Figure 4**). These insect wings have been widely studied as strong, lightweight materials, especially in the context of aerodynamics [32–34]. The wing can be broadly defined as composed of two layers, the procuticle, which is the predominate layer and the epicuticle, which consists of a

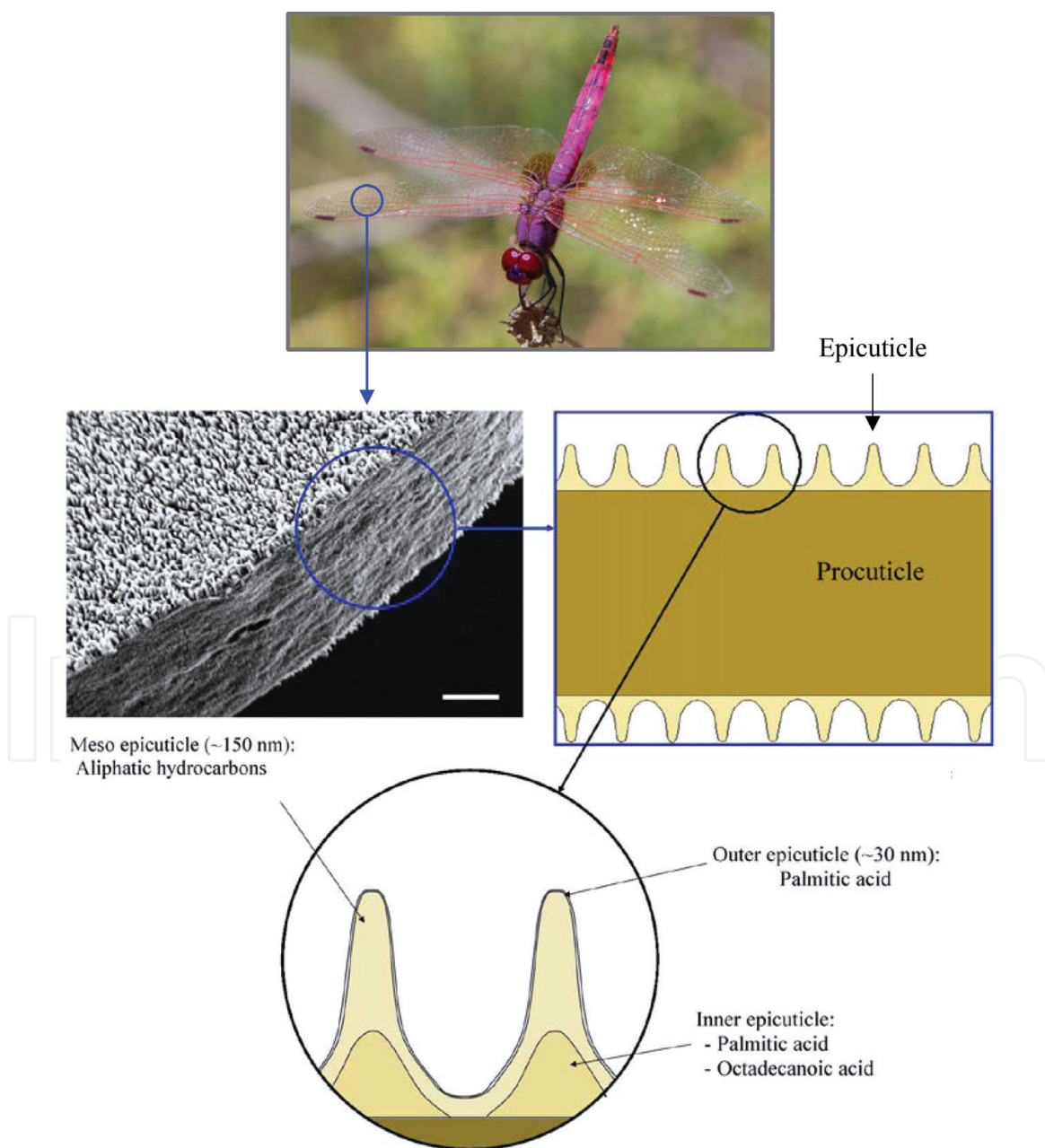


Figure 4. Proposed model of the epicuticle of the dragonfly wing membrane. Three layers are contained within the epicuticle: the outer epicuticle, the meso epicuticle and the inner epicuticle (adapted from Ivanova et al.) [5].

thin layer of nanoscale pillars on both the dorsal and ventral sides of the procuticle and significantly contributes to the surface properties of the wings.

Synchrotron-source IR spectroscopy is useful for investigating the chemical composition of defined areas of materials. IR spectroscopy provides important information of the molecular bonding, groups and structure of chemical identities present in a sample. The extremely intense and collimated light generated enables significantly improved sensitivity, with a low signal-to-noise ratio. Furthermore, the IRM beamline at the Australian Synchrotron is coupled to a Fourier-transform infrared (FTIR) spectrometer and microscope, providing a highly focused IR beam, which enables spatially resolved chemical maps close to the diffraction limit, to be generated pixel by pixel. These properties are advantageous when characterising the chemical composition and distribution of the insect wing membrane, which is only a few microns thick, and possess lateral features on the nano-/microscale. A comparison with other surface chemistry characterisation techniques is made in **Table 1**.

Technique	Insect wing sample	Advantages	Disadvantages	Refs
Synchrotron-source IR spectroscopy	Dragonfly, cicada and damselfly wings	Performed in atmospheric conditions and suitable for sensitive samples Able to map chemical functionality across the wings with high spatial resolution	Does not provide the identity of individual chemical species (only chemical bonding)	[14, 24, 36]
X-ray photoelectron spectroscopy	Dragonfly wings, <i>Hemianax papuensis</i> 15 species of cicadas	Overall chemistry of insect wing surfaces at the top layer Capable of surface excavation to reveal the chemical depth profile	Does not provide details of chemical bonding Unable to map	[35] [37]
Raman microspectroscopy	<i>Drosophila</i> wings	Overall chemical functionality of insect wing surfaces Able to map the wing surfaces with pixel-to-pixel distance less than 1 μm	Low signal-to-noise ratio Interference by the fluorescent background of the insect wings	[38]
MALDI-TOF mass microspectroscopy	Wings of the grey flesh fly (<i>Neobellieria bullata</i>) and common fruit fly (<i>Drosophila melanogaster</i>)	Provides the direct chemical functionality of the insect wing surface Able to map chemical functionality across the insect wings	The samples are required to be completely flat Low spatial resolution Destructive to the sample	[39]

Table 1.

A comparison of different techniques to characterise the surface chemistry of different insect wings.


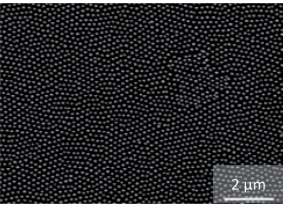
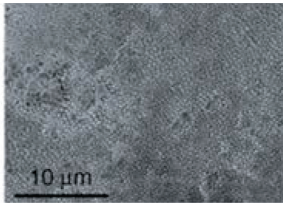
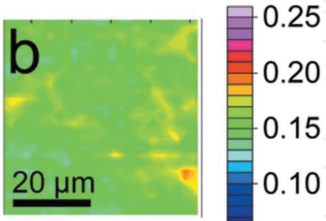

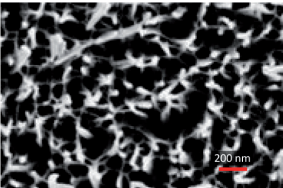
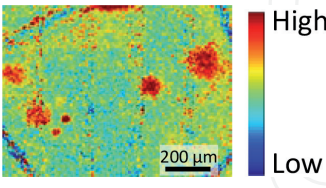
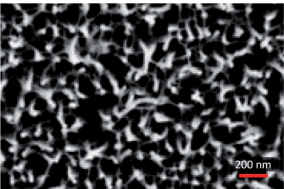
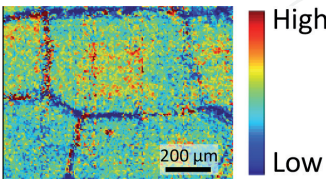
4.1 Transmission mode


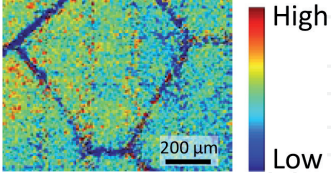
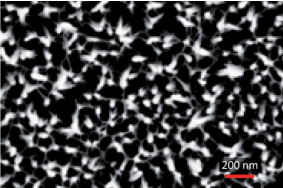
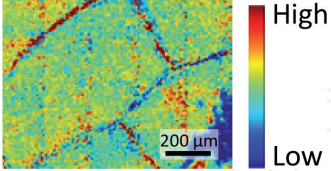
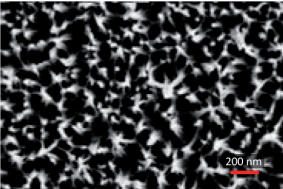
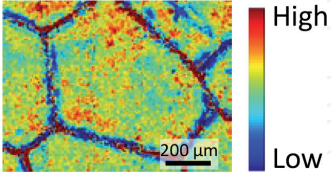
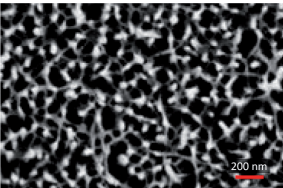
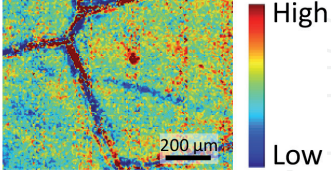

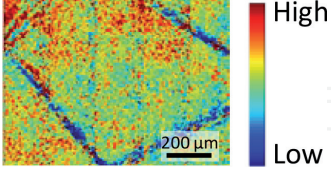
Insect wings were cut into small sections using a sterile surgical blade. Spectra were collected in transmission mode within the 4000–800 cm^{-1} spectral region. High-resolution spectral maps of the wing samples were obtained through FTIR microspectroscopy at the infrared microspectroscopy (IRM) beamline at the Australian Synchrotron. These spectral maps detail spatial variations in peaks representative of lipid components (ester carbonyl $\text{C}=\text{O}$ peak or $\text{C}-\text{H}$ stretching peaks). A comparison of the nanostructures present on the wing membrane surface and lipid spectral maps of different cicada, dragonfly and damselfly species is presented in **Table 2**.

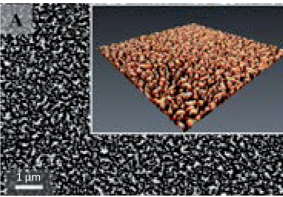
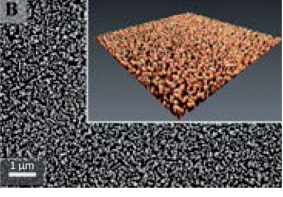
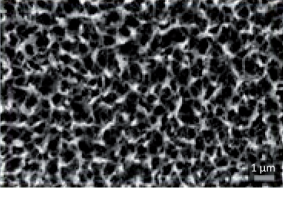
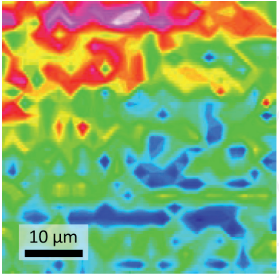
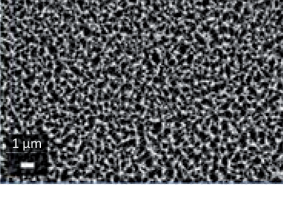
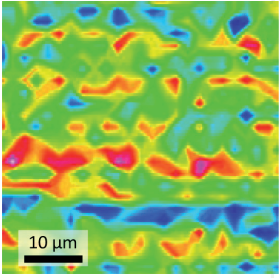
The wing membrane of cicadas, on both the ventral and dorsal sides, consists of a periodic hexagonal array of spherically capped nanopillars [23, 44]. Comparatively, the wing membranes of dragonflies and damselflies are covered with an irregular array of single and clustering nanopillars, which are typically taller with a larger distribution in height than those present on cicada wings.


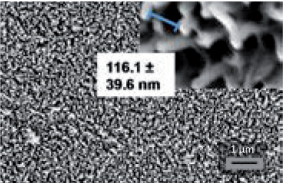
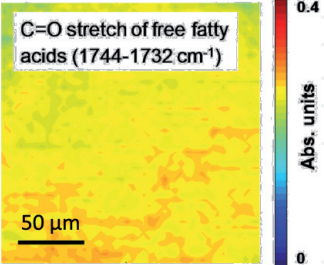
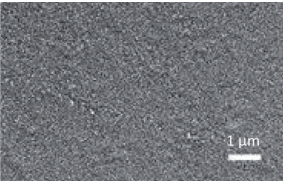
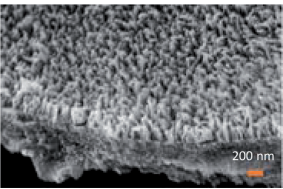
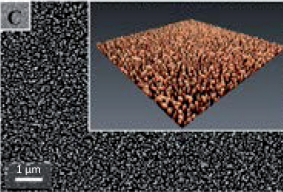
Where provided, the 2D spectral maps of the dragonfly wings showed spatial variations in the intensity of the ester carbonyl peak and $\nu_{\text{as}} \text{CH}_2$ stretching peak, both a characteristic of lipids. Most studies focus on the membrane of the wing, as this is primarily responsible for the unique surface properties of interest. However, Cheeseman et al. [36] use wider fields of view which encompass regions of the vein and membrane where it can be observed that the distribution of lipids was higher in the membrane sections, represented in red, when compared to the wing veins, indicated in blue [36]. Among the dragonfly and damselfly wing samples, the lipid spectral maps appear heterogenous across the surface, often resulting in microdomains of higher concentrations of lipids. This is likely to reflect the unique array of nanopillars, as indicated in the scanning electron micrographs, which tend to cluster. In comparison, the cicada sample appears more homogenous, possibly reflecting the uniform pattern of free-standing nanopillars on the epicuticle.

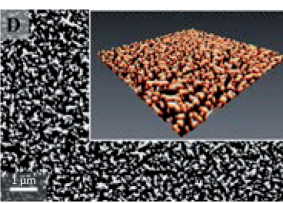
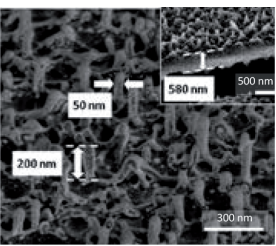
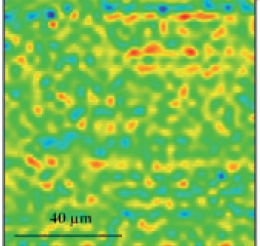
The average spectra from each sample contain three major band groups at 3500–3100 cm^{-1} , 3000–2800 cm^{-1} and 1800–1450 cm^{-1} which correspond to the hydroxyl, alkyl hydrocarbons and ester carbonyl groups, respectively [3, 45, 46]. The presence of $\text{C}-\text{H}$ stretching bands, particularly $\nu_{\text{as}} \text{CH}_2$ and $\nu_{\text{s}} \text{CH}_2$, indicates long-chain aliphatic hydrocarbons typical of waxes [1, 45]. The spectra of all wings were dominated by amide I and amide II absorption bands, due to $\text{C}=\text{O}$ bond stretching coupled to $\text{N}-\text{H}$ bending (1695–1610 cm^{-1}) and $\text{C}-\text{N}$ stretching coupled to $\text{N}-\text{H}$ bending (1575–1480 cm^{-1}), respectively [3]. The presence of these amide groups is attributed to the chitin and protein components of the wings, as they represent the major structural components of the insect cuticle. The $\text{C}-\text{H}$ stretching region (2840–3000 cm^{-1}) represents the symmetric (ν_{s}) and antisymmetric (ν_{as}) stretching vibrations of the CH_2 and CH_3 functional groups. The high proportion of CH_2 stretching bands in comparison to CH_3 , indicates the presence of long-chain aliphatic hydrocarbons [1, 45]. To further understand the top surface layer of the wing membrane, Tobin et al. [14] subtracted spectra extracted from a point of low intensity on the $\nu_{\text{as}} \text{CH}_2$ integration map from a point of high intensity. This was performed in collaboration with the Synchrotron Radiation Center (SRC), University of Wisconsin-Madison, performed at the IRENI Beamline. Following subtraction, the only significant peaks which remained corresponded to $\nu_{\text{s}} \text{CH}_2$ and $\nu_{\text{as}} \text{CH}_2$ vibrations in the $\text{C}-\text{H}$ stretching region, consistent with a long-chain hydrocarbon [14]. An additional approach to identify the top surface layer has been taken in multiple studies, where by spectral measurements were performed on wings following the selective removal of the lipid components using chloroform, demonstrating a reduction of the $\text{C}-\text{H}$ stretching bands [14, 35, 41]. The intensity of these $\text{C}-\text{H}$ stretching bands varied between the insects (**Figure 5**). The cicada

Insect group	Species	Physical structure	Lipid spectral map*
Cicada			
 <p data-bbox="199 505 244 532">[14]</p>	<i>Psaltoda claripennis</i> [23]	 <p data-bbox="1124 521 1168 548">2 μm</p>	No data available
	<i>Psaltoda claripennis</i> ^a [14]	 <p data-bbox="919 764 987 792">10 μm</p>	 <p data-bbox="1437 626 1477 670">b</p> <p data-bbox="1437 764 1528 808">20 μm</p> <p data-bbox="1672 602 1754 805">0.25 0.20 0.15 0.10</p>
Dragonfly			
 <p data-bbox="199 1065 244 1092">[40]</p>	<i>Austrothemis nigrescens</i> ^b [36]	 <p data-bbox="1107 1078 1152 1105">200 nm</p>	 <p data-bbox="1672 932 1754 1118">High Low</p> <p data-bbox="1578 1078 1646 1105">200 μm</p>
	<i>Orthetrum chrysostigma</i> ^b [36]	 <p data-bbox="1107 1317 1152 1344">200 nm</p>	 <p data-bbox="1672 1162 1754 1349">High Low</p> <p data-bbox="1578 1300 1646 1328">200 μm</p>

Insect group	Species	Physical structure	Lipid spectral map*
	<i>Trithemis annulata</i> ^b [36]		
	<i>Sympetrum fonscolombii</i> ^b [36]		
	<i>Anax parthenope</i> ^b [36]		
	<i>Anax imperator</i> ^b [36]		
	<i>Onychogomphus forcipatus</i> ^b [36]		

Insect group	Species	Physical structure	Lipid spectral map*
	<i>Diplacodes melanopsis</i> [7]		No data available
	<i>Diplacodes bipunctata</i> [7]		No data available
	<i>Hemianax papuensis</i> ^c [35]		
	<i>Hemicordulia tau</i> ^c [41]		

Insect group	Species	Physical structure	Lipid spectral map*
Damselfly  [42]	<i>Calopteryx haemorrhoidalis</i> [24]		
	<i>Calopteryx haemorrhoidalis</i> [26]		No data available
	<i>Calopteryx haemorrhoidalis</i> [25]		No data available
	<i>Xanthagrion erythroneurum</i> [7]		No data available

Insect group	Species	Physical structure	Lipid spectral map [*]
	<i>Ischnura heterosticta</i> [7]		No data available
	<i>Ischnura heterosticta</i> [43]		

^{*}With the exception of the second entry (*Psaltoda claripennis*), the lipid spectral maps were generated by integrating the ester carbonyl peak, approximately in the wavelength range 1750–1720 cm^{-1} , which is representative of the C=O stretch of esters

^aLipid spectral map generated by the absorbance under the ν_{as} CH_2 : 2931–2913 cm^{-1}

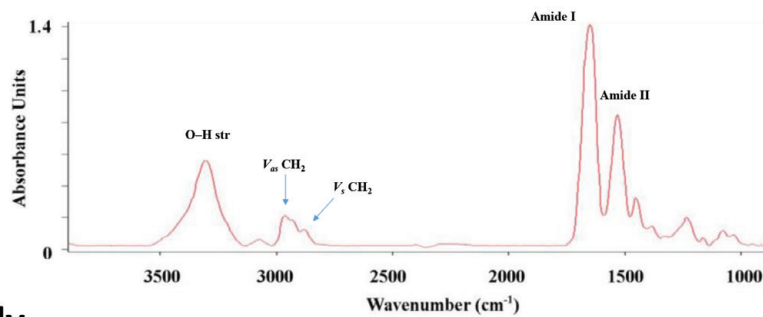
^bSpectral data in Cheeseman et al. [36] was collected using an offline Globar™ IR source at the IRM beamline at the Australian Synchrotron

^cLipid spectral maps for *Hemianax papuensis* and *Hemicordulia tau* are unpublished and were generated by integrating the ester carbonyl peak, approximately in the wavelength range 1750–1720 cm^{-1}

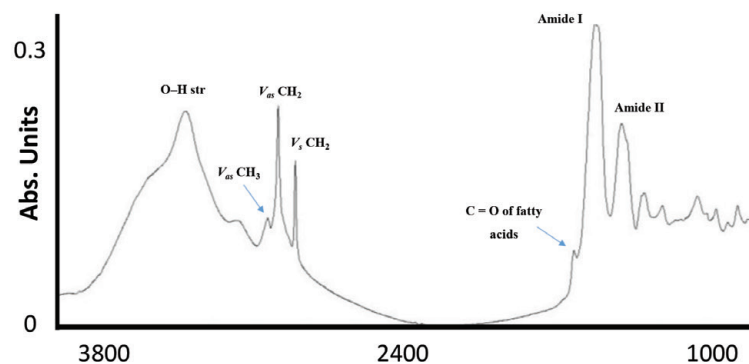
Table 2.

A comparison of the nanostructures present on the wing membrane surface of different cicada, dragonfly and damselfly species and high-resolution lipid spectral maps generated using IR microspectroscopy.

Cicada



Dragonfly



Damselfly

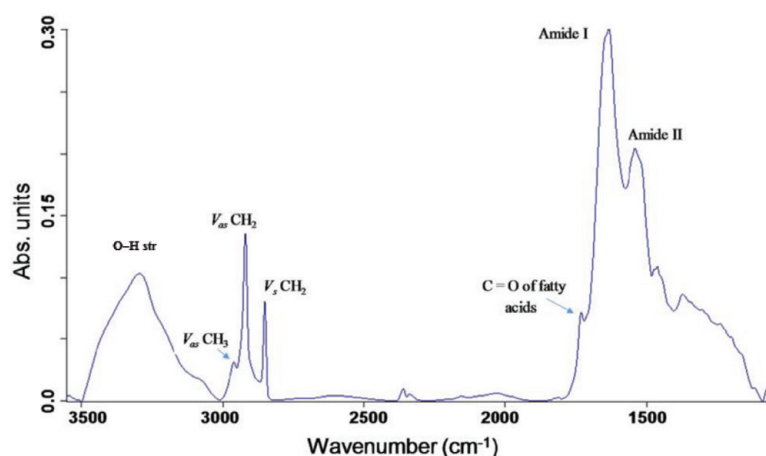


Figure 5. Average IR spectra of an area of the wing membrane of a species of cicada (*Psaltoda claripennis*), (adapted from Ivanova et al. [23]), reprinted with permission from John Wiley and Sons, dragonfly (*Austrothemis nigrescens*) (adapted from Cheeseman et al. [36]) and damselfly (*Calopteryx haemorrhoidalis*) (adapted from Truong et al. [24]), both reprinted with permission from Springer.

wing sample demonstrated comparatively lower peaks in the C—H stretching region than the dragonfly and damselfly wing samples, which may reflect the reduced height of the waxy nanopillars on the cicada (~200 nm) compared to the dragonfly (~200–300 nm) and damselfly (~400–500 nm).

4.2 Transmission versus attenuated total reflectance

In addition to transmission mode, there is also attenuated total reflectance (ATR) mode available at the Australian Synchrotron. This mode utilises a Ge crystal with a high refractive index, through an in-house-developed device, generating an evanescent wave penetrating only the top surface layer of the sample, as described above. The high refractive index promotes detection of molecular bonding in very small concentrations in the sample. This mode is advantageous to transmission for thick or opaque samples, where transmission is not achievable or in circumstances

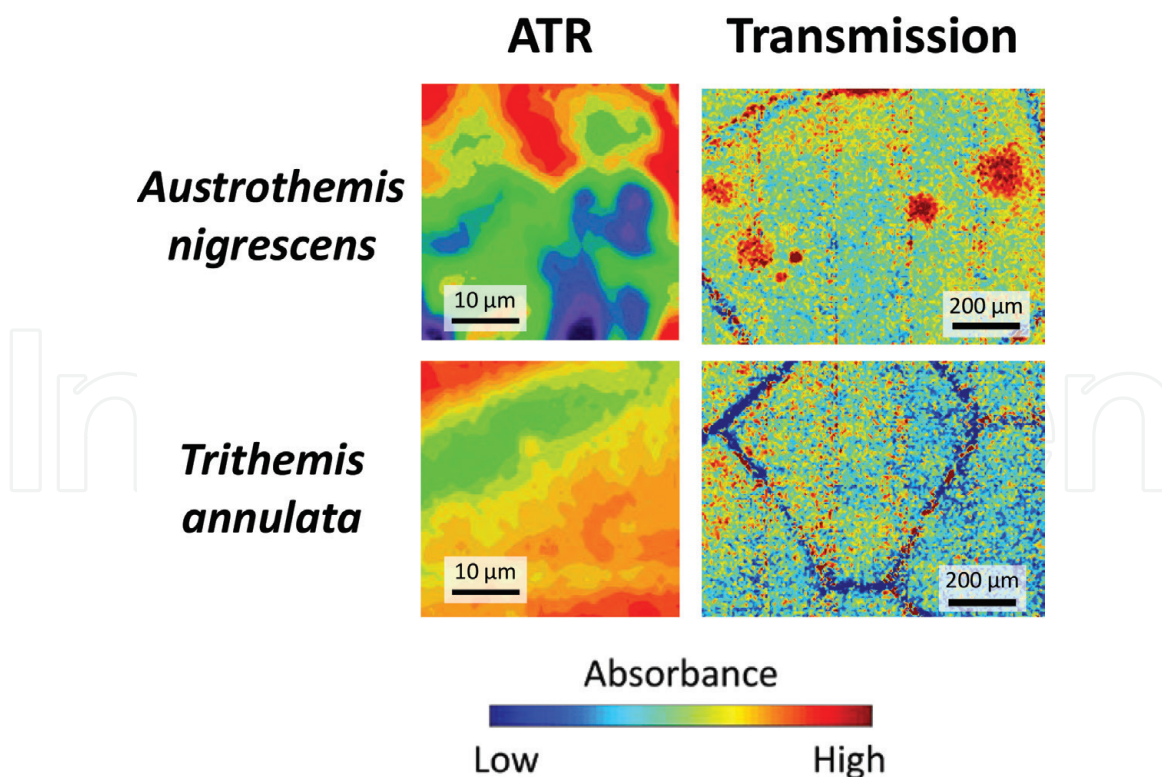


Figure 6. Comparison of the distribution of lipid components of the wing membrane of two dragonflies, *A. nigrescens* and *T. annulata*, acquired using ATR (unpublished) and transmission (adapted from Cheeseman et al. [36]) mode IR spectroscopy at the Australian Synchrotron. Lipid spectral maps were generated by integrating the ester carbonyl peak, in the wavelength range $1750\text{--}1720\text{ cm}^{-1}$, which is representative of the C=O stretch of esters.

when only the top surface of the sample is of interest. In the case of characterising insect wing membranes, ATR mode provides a complimentary technique to transmission, generating high-resolution spectral maps of only the top surfaces (primarily epicuticle), which is of interest as the primary contributor to the unique anti-wetting, anti-biofouling and bactericidal properties. A comparison of spectral maps generated from ATR and transmission mode of the wings of two dragonflies is presented in **Figure 6**.

The high spatial resolution of ATR IR spectroscopy demonstrates the lateral distributions of lipids/waxes on the micron scale (**Figure 6**). Additionally, because the light source only partially penetrates the surface in ATR mode, the spectral map more closely represents the lipid distribution on the wing epicuticle, composed of an irregular array of lipid nanopillars. However, there is also a compromise as structural details of the procuticle are not included and the total imaging area is limited to the facet size of the crystal. Additionally, because ATR mode requires physical contact between the crystal and the sample surface, image quality is affected by the topography of the surface, with issues arising with non-flat surfaces. For example, it is not possible to image both the vein and membrane sections of the dragonfly wings due to the large height difference between the membrane and vein surface.

5. Conclusions

The use of synchrotron-source infrared (IR) spectroscopy is an effective method of surface characterisation to determine the chemical composition across insect wings. The intense and highly collimated light source allows sensitive detection of chemical components with high-resolution spatial mapping. Such sensitive surface

characterisation is useful for insect wings, as well as other natural materials with unique surface properties, which may have important applications as templates for biomedical, environmental or industrially relevant materials.

Acknowledgements

This research was undertaken in part on the IRM beamline at Australian Synchrotron (Victoria, Australia), part of ANSTO. The development of the macro ATR-FTIR device mentioned here was funded as part of the Science Projects at the Australian Synchrotron and has been made available to users of the IRM beamline. The authors wish to acknowledge Mr. Alan Easdon from the Australian Synchrotron, for his substantial contribution to the design and mechanical works associated with the development of this device.

Conflict of interest

The authors declare no conflicts of interest in this work.

Author details

Samuel Cheeseman¹, Vi Khanh Truong¹, Jitraporn Vongsvivut², Mark J. Tobin², Russell Crawford¹ and Elena P. Ivanova^{1*}

¹ School of Science, College of Science, Engineering and Health, RMIT University, Melbourne, Australia

² Infrared Microspectroscopy (IRM) Beamline, Australian Synchrotron, ANSTO, Clayton, Victoria, Australia

*Address all correspondence to: elena.ivanova@rmit.edu.au

IntechOpen

© 2019 The Author(s). Licensee IntechOpen. This chapter is distributed under the terms of the Creative Commons Attribution License (<http://creativecommons.org/licenses/by/3.0>), which permits unrestricted use, distribution, and reproduction in any medium, provided the original work is properly cited. 

References

- [1] Coates J. Interpretation of infrared spectra, a practical approach. In: Meyers RA, McKelvy ML, editors. Encyclopedia of Analytical Chemistry. Chichester, England: Wiley & Sons; 2000. pp. 10815-10837
- [2] Vongsvivut J, Heraud P, Gupta A, Puri M, McNaughton D, Barrow CJ. FTIR microspectroscopy for rapid screening and monitoring of polyunsaturated fatty acid production in commercially valuable marine yeasts and protists. *The Analyst*. 2013;**138**(20):6016-6031. DOI: 10.1039/c3an00485f
- [3] Barth A. Infrared spectroscopy of proteins. *Biochimica et Biophysica Acta (BBA)-Bioenergetics*. 2007;**1767**(9):1073-1101. DOI: 10.1016/j.bbabi.2007.06.004
- [4] Bandara CD, Singh S, Afara IO, Wolff A, Tesfamichael T, Ostrikov K, et al. Bactericidal effects of natural nanotopography of dragonfly wing on *Escherichia coli*. *ACS Applied Materials & Interfaces*. 2017;**9**(8):6746-6760. DOI: 10.1021/acsami.6b13666
- [5] Ivanova EP, Hasan J, Webb HK, Gervinskis G, Juodkazis S, Truong VK, et al. Bactericidal activity of black silicon. *Nature Communications*. 2013;4:2838-42844. DOI: 10.1038/ncomms3838
- [6] Mainwaring DE, Nguyen SH, Webb H, Jakubov T, Tobin M, Lamb RN, et al. The nature of inherent bactericidal activity: Insights from the nanotopology of three species of dragonfly. *Nanoscale*. 2016;**8**(12):6527-6534. DOI: 10.1039/C5NR08542J
- [7] Nguyen SH, Webb HK, Hasan J, Tobin MJ, Mainwaring DE, Mahon PJ, et al. Wing wettability of odonata species as a function of quantity of epicuticular waxes. *Vibrational Spectroscopy*. 2014;**75**(Supplement C):173-177. DOI: 10.1016/j.vibspec.2014.07.006
- [8] Song Ha N, Hayden KW, Peter JM, Russell JC, Elena PI. Natural insect and plant micro-/nanostructured surfaces: An excellent selection of valuable templates with superhydrophobic and self-cleaning properties. *Molecules*. 2014;**19**(9):13614-13630. DOI: 10.3390/molecules190913614
- [9] Gangadoo S, Chandra S, Power A, Hellio C, Watson GS, Watson JA, et al. Biomimetics for early stage biofouling prevention: Templates from insect cuticles. *Journal of Materials Chemistry B*. 2016;**4**(34):5747-5754. DOI: 10.1039/C6TB01642A
- [10] Tiller JC, Liao C-J, Lewis K, Klibanov AM. Designing surfaces that kill bacteria on contact. *Proceedings of the National Academy of Sciences of the United States of America*. 2001;**98**(11):5981-5985. DOI: 10.1073/pnas.111143098
- [11] Pacor S, Giangaspero A, Bacac M, Sava G, Tossi A. Analysis of the cytotoxicity of synthetic antimicrobial peptides on mouse leucocytes: Implications for systemic use. *Journal of Antimicrobial Chemotherapy*. 2002;**50**(3):339-348. DOI: 10.1093/jac/dkf141
- [12] Mijndonckx K, Leys N, Mahillon J, Silver S, Van Houdt R. Antimicrobial silver: Uses, toxicity and potential for resistance. *Biometals*. 2013;**26**(4):609-621. DOI: 10.1007/s10534-013-9645-z
- [13] Stapleton PD, Taylor PW. Methicillin resistance in *Staphylococcus aureus*: Mechanisms and modulation. *Science Progress*. 2002;**85**(1):57-72. DOI: 10.3184/003685002783238870
- [14] Tobin MJ, Puskar L, Hasan J, Webb HK, Hirschmugl CJ, Nasse MJ,

et al. High-spatial-resolution mapping of superhydrophobic cicada wing surface chemistry using infrared microspectroscopy and infrared imaging at two synchrotron beamlines. *Journal of Synchrotron Radiation*. 2013;20(3):482-489. DOI: 10.1107/S0909049513004056

[15] Caine S, Heraud P, Tobin MJ, McNaughton D, Bernard CCA. The application of Fourier transform infrared microspectroscopy for the study of diseased central nervous system tissue. *NeuroImage*. 2012;59(4):3624-3640. DOI: 10.1016/j.neuroimage.2011.11.033

[16] Miller LM, Dumas P. Chemical imaging of biological tissue with synchrotron infrared light. *Biochimica et Biophysica Acta (BBA)—Biomembranes*. 2006;1758(7):846-857. DOI: 10.1016/j.bbamem.2006.04.010

[17] Benbow NL, Webber JL, Pawlitzak P, Sebben DA, Ho TTMV, Vongsvivut J, et al. A novel soft contact piezo-controlled liquid cell for probing polymer films under confinement using synchrotron FTIR microspectroscopy. *Scientific Reports*. 2019. In press

[18] Dorakumbura BN, Boseley RE, Becker T, Martin DE, Richter A, Tobin M, et al. Revealing the spatial distribution of chemical species within latent fingerprints using vibrational spectroscopy. *The Analyst*. 2018;143:4027-4039. DOI: 10.1039/C7AN01615H

[19] Timilsena YP, Vongsvivut J, Tobin MJ, Adhikari R, Barrow C, Adhikari B. Investigation of oil distribution in spray-dried chia seed oil microcapsules using synchrotron-FTIR microspectroscopy. *Food Chemistry*. 2019;275457-275466. DOI: 10.1016/j.foodchem.2018.09.043

[20] Ryu M, Balçytis A, Wang X, Vongsvivut J, Hikima Y, Li J, et al.

Orientational mapping augmented sub-wavelength hyper-spectral imaging of silk. *Scientific Reports*. 2017;7(1):7419. DOI: 10.1038/s41598-017-07502-3

[21] Nunna S, Creighton C, Fox BL, Naebe M, Maghe M, Tobin MJ, et al. The effect of thermally induced chemical transformations on the structure and properties of carbon fibre precursors. *Journal of Materials Chemistry A*. 2017;5(16):7372-7382. DOI: 10.1039/C7TA01022B

[22] Vongsvivut J, Truong VK, Al Kobaisi M, Maclaughlin S, Tobin MJ, Crawford RJ, et al. Synchrotron macro ATR-FTIR microspectroscopic analysis of silica nanoparticle-embedded polyester coated steel surfaces subjected to prolonged UV and humidity exposure. *PLoS One*. 2017;12(12):e0188345. DOI: 10.1371/journal.pone.0188345

[23] Ivanova EP, Hasan J, Webb HK, Truong VK, Watson GS, Watson JA, et al. Natural bactericidal surfaces: Mechanical rupture of *Pseudomonas aeruginosa* cells by cicada wings. *Small*. 2012;8(16):2489-2494. DOI: 10.1002/sml.201200528

[24] Truong VK, Geeganagamage NM, Baulin VA, Vongsvivut J, Tobin MJ, Luque P, et al. The susceptibility of *Staphylococcus aureus* CIP 65.8 and *Pseudomonas aeruginosa* ATCC 9721 cells to the bactericidal action of nanostructured *Calopteryx haemorrhoidalis* damselfly wing surfaces. *Applied Microbiology and Biotechnology*. 2017;101(11):4683-4690. DOI: 10.1007/s00253-017-8205-9

[25] Stuhr S, Truong VK, Vongsvivut J, Senkbeil T, Yang Y, Al Kobaisi M, et al. Structure and chemical organization in damselfly *Calopteryx haemorrhoidalis* wings: A spatially resolved FTIR and XRF analysis with synchrotron radiation. *Scientific Reports*. 2018;8(1):8413. DOI: 10.1038/s41598-018-26563-6

- [26] Truong VK, Vongsvivut J, Mahanamanam N, Tobin MJ, Luque P, Baulin V, et al. Study of melanin localization in the mature male *Calopteryx haemorrhoidalis* damselfly wings. *Journal of Synchrotron Radiation*. 2018;**25**(3):874-877. DOI: 10.1107/S1600577518004460
- [27] Harrick NJ. *Internal Reflection Spectroscopy*. NY: John Wiley & Sons; 1967
- [28] Truong VK, Stefanovic M, Maclaughlin S, Tobin M, Vongsvivut J, Al Kobaisi M, et al. The evolution of silica nanoparticle-polyester coatings on surfaces exposed to sunlight. *Journal of Visualized Experiments*. 2016:e54309
- [29] Bhadra CM, Truong VK, Pham VT, Al Kobaisi M, Seniutinas G, Wang JY, et al. Antibacterial titanium nano-patterned arrays inspired by dragonfly wings. *Scientific Reports*. 2015:516817. DOI: 10.1038/srep16817
- [30] Hasan J, Raj S, Yadav L, Chatterjee K. Engineering a nanostructured “super surface” with superhydrophobic and superkilling properties. *RSC Advances*. 2015;**5**(56):44953-44959. DOI: 10.1039/C5RA05206H
- [31] Linklater DP, Nguyen HKD, Bhadra CM, Juodkasis S, Ivanova EP. Influence of nanoscale topology on bactericidal efficiency of black silicon surfaces. *Nanotechnology*. 2017;**28**(24):245301. DOI: 10.1088/1361-6528/aa700e
- [32] Appel E, Heepe L, Lin C-P, Gorb SN. Ultrastructure of dragonfly wing veins: Composite structure of fibrous material supplemented by resilin. *Journal of Anatomy*. 2015;**227**(4):561-582. DOI: 10.1111/joa.12362
- [33] Sivasankaran PN, Ward TA, Viyapuri R, Johan MR. Static strength analysis of dragonfly inspired wings for biomimetic micro aerial vehicles. *Chinese Journal of Aeronautics*. 2016;**29**(2):411-423. DOI: 10.1016/j.cja.2016.02.007
- [34] Jongerius SR, Lentink D. Structural analysis of a dragonfly wing. *Experimental Mechanics*. 2010;**50**(9):1323-1334. DOI: 10.1007/s11340-010-9411-x
- [35] Ivanova EP, Nguyen SH, Webb HK, Hasan J, Truong VK, Lamb RN, et al. Molecular organization of the nanoscale surface structures of the dragonfly *Hemianax papuensis* wing epicuticle. *PLoS One*. 2013;**8**(7):e67893. DOI: 10.1371/journal.pone.0067893
- [36] Cheeseman S, Owen S, Truong VK, Meyer D, Ng SH, Vongsvivut J, et al. Pillars of life: Is there a relationship between lifestyle factors and the surface characteristics of dragonfly wings? *ACS Omega*. 2018;**3**(6):6039-6046. DOI: 10.1021/acsomega.8b00776
- [37] Sun M, Watson GS, Zheng Y, Watson JA, Liang A. Wetting properties on nanostructured surfaces of cicada wings. *Journal of Experimental Biology*. 2009;**212**(19):3148-3155. DOI: 10.1242/jeb.033373
- [38] Valmalette JC, Raad H, Qiu N, Ohara S, Capovilla M, Robichon A. Nano-architecture of gustatory chemosensory bristles and trachea in *Drosophila* wings. *Scientific Reports*. 2015:514198. DOI: 10.1038/srep14198
- [39] Vrkoslav V, Muck A, Cvačka J, Svatoš A. MALDI imaging of neutral cuticular lipids in insects and plants. *Journal of the American Society for Mass Spectrometry*. 2010;**21**(2):220-231. DOI: 10.1016/j.jasms.2009.10.003
- [40] Hort J, Hort F. *Austrothemis nigrescens* [Image]. 2011. Available from: http://eol.org/data_objects/31719003 [Accessed: 01/11/2018]
- [41] Nguyen SHT, Webb HK, Hasan J, Tobin MJ, Crawford RJ, Ivanova EP.

Dual role of outer epicuticular lipids in determining the wettability of dragonfly wings. *Colloids and Surfaces B: Biointerfaces*. 2013;106126-106134. DOI: 10.1016/j.colsurfb.2013.01.042

[42] Hampshire G. *Calopteryx haemorrhoidalis* [Image]. 2013. Available from: <http://eol.org/pages/4139774/overview> [Accessed: 01/11/2018]

[43] Hasan J, Webb HK, Truong VK, Watson GS, Watson JA, Tobin MJ, et al. Spatial variations and temporal metastability of the self-cleaning and superhydrophobic properties of damselfly wings. *Langmuir*. 2012;28(50):17404-17409. DOI: 10.1021/la303560w

[44] Watson GS, Myhra S, Cribb BW, Watson JA. Putative functions and functional efficiency of ordered cuticular nanoarrays on insect wings. *Biophysical Journal*. 2008;94(8):3352-3360. DOI: 10.1529/biophysj.107.109348

[45] Coury C, Dillner AM. A method to quantify organic functional groups and inorganic compounds in ambient aerosols using attenuated total reflectance FTIR spectroscopy and multivariate chemometric techniques. *Atmospheric Environment*. 2008;42(23):5923-5932. DOI: 10.1016/j.atmosenv.2008.03.026

[46] Lasch P, Boese M, Pacifico A, Diem M. FT-IR spectroscopic investigations of single cells on the subcellular level. *Vibrational Spectroscopy*. 2002;28(1):147-157. DOI: 10.1016/S0924-2031(01)00153-9